USING THE HIGH RESOLUTION AND DYNAMICS LIMB SOUNDER (HIRDLS) TO WARN AVIATION OF VOLCANIC ASH

R. G. Grainger and J. J. Barnett

Atmospheric, Oceanic and Planetary Physics
Department of Physics
University of Oxford

August 1997

Contents

Abstract

Between 1980 and 1994 eighty jet airplanes have been damaged by unplanned encounters with drifting clouds of volcanic ash in air routes and at airports. It is expected that this average rate of 5.3 encounters per year is increasing with increased air traffic, however the natural variability of volcanism implies that there will be high year-to-year variability about the trend.

Ash clouds which are a hazard to aircraft have radar reflectivity several orders of magnitude smaller than the reflectivity for severe weather so do not appear on on-board radar. Visual recognition of a volcanic hazard may be difficult at night or during the day as ash clouds commonly look like normal weather clouds.

The International Civil Aviation Organization (ICAO) has set up a network of Volcanic Ash Alert Centres (VAACs), to provide forecasts of ash cloud dispersion to the civil aviation industry. This report investigates the possibility of using satellite instrumentation to identify hazardous volcanic clouds and so provide a real time warning to air traffic.

Of the many proposed and operational satellite instruments many have to be discounted because they do not have the ability to discriminate normal water and ice clouds from freshly formed volcanic clouds. In addition several instruments take days or even months to sample volcanic locations and so could miss a significant volcanic event. Limb sounders are particularly promising because they can geometrically distinguish ice or water clouds from higher ash clouds. In particular the High Resolution Dynamics Limb Sounder (HIRDLS) is a multispectral instrument which measures atmospheric emission so it can operate during both day and night. The measurements in 21 spectral channels provide an alternative method to identify cloud type.

The conclusions of the report are:

i) There are concerns about HIRDLS pixel size, and to what extent ash clouds would fall between pixels; this would effectively reduce the sampling interval for a given location from 12 hours to perhaps 24, 36 or 48 hours. Nevertheless HIRDLS could provide flight path hazard proximity warnings for a long-lived moderate to large ash cloud.

ii) Study of the spectral properties shows that very young ash (<12 hours) may have a particle size distribution that makes discrimination from meteorological clouds more difficult than previously thought. This should have a more serious effect on vertical imager 'two-colour' techniques than on HIRDLS data, since the latter benefits also from using geometry to identify stratospheric ash. Hence on balance, this makes the HIRDLS data more useful than previously thought for the stratosphere, but in the troposphere, it means that both limb and vertical view data are less useful (and probably explains past problems with vertical view data).

iii) Ash warnings based on HIRDLS data would be most effectively distributed through the standard ICAO warning system.

iv) Joint retrieval of HIRDLS data with those from other satellite sensors is not viable, and any combined use of data would have to be performed at high level by human effort.

1 Volcanic Eruptions

1.1 Introduction

Linear belts of volcanoes are a striking feature of the Earth and they reflect, in most cases, movement of the major tectonic plates that make up the Earth's outer shell. Where plates coverage (typically at speeds of a few centimeters per year) the thinner plate is normally thrust down under the thicker and melts in the hot subcrustal environment. Liquid rock is less dense than solid rock so magma (molten or liquid rock) migrates towards the surface. The resulting subduction volcanism is usually both explosive, near to or on land and is reasonably well documented. Rift volcanism occurs where plates spread apart and is characterized by the relatively non-explosive outpouring of lava and commonly takes place on or below the ocean's surface. The records of rift volcanism are incomplete, being dominated by those few regions where the spreading apart of plates takes place above sea level such as in East Africa and Iceland. Intraplate volcanism occurs within the major plates and is associated with relatively hot subcrustal regions. The record of intraplate volcanism is better than that for rift volcanism but many volcanoes are probably unrecorded, particularly those on the sea floor. In an analysis of 5337 historical eruptions 87 % were subduction, 9 % intraplate and 4 % rift generated (Simkin and Siebert, 1994). Of the approximately 4 km^3 of material produced by volcanoes annually, the majority, 78 %, is from rift volcanoes, with intraplate and subduction volcanoes accounting for the remainder (about 11 % of the total each).

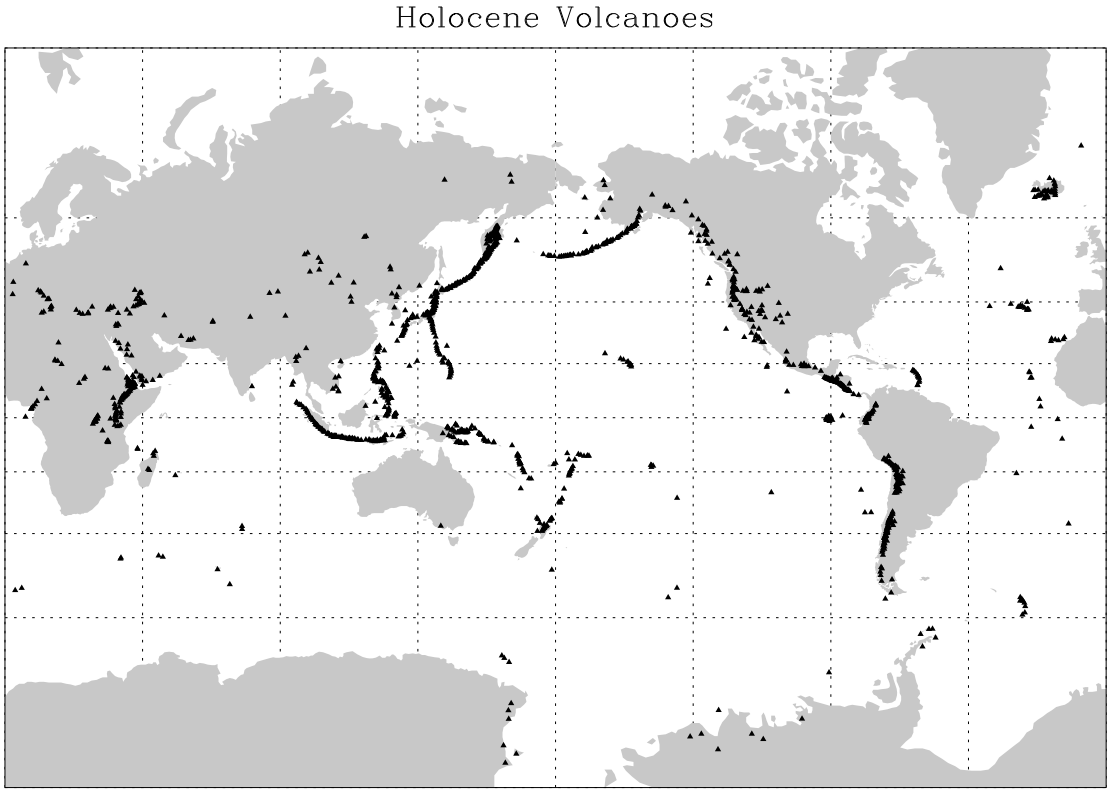

Figure 1: Location of volcanoes thought to have been active in the last 10, 000 years (Holocene). Volcanic belts cover 0.6 % of the Earth's surface. *Source, Smithsonian Institution, Global Volcanism Program.*

Figure 1 shows the location of 1509 volcanoes thought to have been active in the last 10, 000 years (Holocene). Two thirds of the volcanoes are in the northern hemisphere and only one fifth are located between 10 °S and the South Pole. There is no significant concentration of volcanoes with longitude, but over 1000 volcanoes (two thirds of those displayed) lie on the Pacific Ocean margin forming the 'Ring of Fire'.

Approximately 30 % of volcanoes are within 1000 m of sea level, 60 % are within 2 km and about 80 % are within 3000 m.

A volcanic event occurs when there is a sudden or continuing release of energy caused by near-surface or surface magma movement and can include:

- an eruptive pulse, essentially an explosion with an eruption plume, but also non-explosive surges of lava. A pulse may last a few seconds to minutes,
- an eruptive phase that may last a few hours to days and consists of numerous eruptive pulses that may alternate between explosions and lava surges, and
- a single eruption or eruptive episode, composed of several phases, that may last a few days, months or years (Fisher and Schmincke, 1994).

Volcanic eruptions and eruptive phases are traditionally classified according to a wide range of qualitative criteria: the principle eruption types are described in Table 1. Eruption duration can range from a few minutes to thousands of years, with the median duration being 7 weeks (Simkin and Siebert, 1994). Volcanic ash clouds can be produced in extremely small eruptions (in terms of total ashfall mass) of duration less than 1 minute. Violent eruptions commonly occur after long periods of repose, so dangerous volcanoes may not be currently recognized as active. Of the 16 largest explosive eruptions in the last 200 years, 12 were the first historic eruption known from the volcano.

Type	Eruption Height	Magma	Explosive activity	Effusive activity	Ejecta
Hawaiian	$<$ 0.1 - 5 km	fluid	very weak ejection of fluid blobs	often extensive flows	cow-dung bombs and spatter, very little ash
Strombolian	0.1 - 2 km	moderately fluid	weak to violent ejection of pasty fluid blebs	thicker, less extensive flows; flows may be absent	spherical to fusiform bombs; cinder; small to large amounts of glassy ash
Vulcanian	0.3 - 3 km	viscous	moderate to violent ejection of solid hot fragments of new lava	flows commonly absent, thick and stubby if present, ash flows rare	essential, glassy to lithic, blocks and ash, pumice
Plinian	10 - 40 km (hydrovolcanic 20 - 50 km)	viscous	ejection of large volumes of ash, with accompanying caldera collapse	ash flows, small to very luminous; may be absent	glassy ash and pumice
Gas Eruptions		no magma	continuous or rhythmic gas release at vent	none	none or very minor amounts of ash

Table 1: Classification of volcanic eruptions (after http://volcano.und.nodak.edu/vwdocs/vwlessons/kinds/-classification.html). The ash column from all but gas eruption can easily attain 8 km, with the largest potential hazard to aviation coming from Plinian and Vulcanian eruptions. In addition co-ignimbrite ash columns can arise entirely from convective thrust having no gas thrust region.

During a single eruption, styles of activity and types of products may change within minutes or hours, depending upon changes in magma composition, volatiles, or other magma chamber and vent conditions. The diversity of volcanoes and volcanic products is due to differences in the composition of the magma (molten or liquid rock) which controls its viscosity and gas content. Gas becomes less soluble in magma as it approaches the surface and the pressure decreases. The greater the gas content of a magma, the more explosive the eruption.

Magmas rich in silica are more viscous than those poorer in silica. The nomenclature of volcanic rocks depends on the amount of silica (measured as silica oxide, SiO_2) present (see Table 2).

SiO_2 Content	Volcanic Name	Plutonic Name	Description	Viscosity	General Colour
< 53 %	Basalt	Gabbro	mafic	low	dark
53-70 %	Andesite	Diorite	intermediate	intermediate	intermediate
> 70 %	Rhyolite	Granite	felsic	high	light

Table 2: Classification of rock type by SiO_2 content.

1.2 Volcanic Plume and Ash Cloud

In addition to the release of a number of gases an explosive eruption blasts molten and solid rock fragments (tephra) into the air. The largest fragments (bombs) fall back to the ground near the vent, usually within 2 miles. The smallest rock fragments (ash) continue rising into the air, forming an eruption column.

An eruption column consists of three dynamic regions: a basal gas-thrust region, a central buoyant convective region, and an upper umbrella-cloud region where the column spreads out at its level of neutral buoyancy. Eruption columns can grow rapidly, reaching more than 20 km above a volcano in less than 30 minutes. The upper surface of the eruption cloud may be tens of degrees colder than the surrounding environment owing to inertial overshoot of the erupted mixture above the neutral buoyancy height (Woods and Kienle, 1994). This can complicate the estimation of cloud height from thermal satellite imagery.

Analysis of the Geostationary Meteorological Satellite (GMS) and Advanced Very High Resolution Radiometer (AVHRR) images of the Mt Pinatubo eruption plume by Holasek et al. (1996) gave the initial plume radius as 50 km which increased to about 275 km after about 2 hours 45 minutes. Woods and Kienle (1994) state that the 18 May 1980 Mt St Helens ash plume increased in radius from 20 km to 50 km in about 10 minutes. It also took about 10 minutes for the 21 April 1990 Redoubt Volcano plume to increase in radius from about 6 km to over 15 km.

After its initial expansion the ash cloud drifts following the local wind patterns, becoming separated from the volcanic source. The rates of drift of ash clouds are typically in the range of 20 – 100 km hr^{-1}. Vertical wind shear may result in the cloud moving in different directions as a function of altitude. This happened following the March 28th 1982 eruption of El Chichón when the tropospheric component of the ash cloud spread in a north-easterly direction whereas the stratospheric component moved to the southwest (Matson, 1984).

Sawada (1994) tabulates the dimensions (length $\times$ width) of 17 volcanic plumes and ash clouds detected using the GMS from December 1977 to June 1991. These clouds had a typical area equivalent radius of about 110 km with the largest being the 14 – 15 June 1991 Mt Pinatubo cloud which had an area equivalent radius of about 1230 km.

1.2.1 Volcanic Gases

The most common gases associated with active volcanoes are water vapor (90%), carbon dioxide, sulphur dioxide, hydrogen sulphide, hydrogen, helium, carbon monoxide, and hydrochloric acid. Lesser amounts of hydrofluoric acid, nitrogen, argon, and other compounds are also commonly emitted by active volcanoes. Sulphur dioxide gas oxidizes in the atmosphere to form sulphuric acid. This process is relatively slow with an e-folding reaction time of about 35 days (Read et al., 1993). Bluth et al. (1992) were able to observe the movement of the SO_2 cloud from the 1991 Mt Pinatubo eruption for two weeks following the eruption. The sulphuric acid created from the SO_2 condenses into drops which, for sufficiently high injection altitudes (i.e. stratospheric), may remain aloft for several years.

1.2.2 Pyroclasts

The term pyroclastic is used to refer to volcanic materials ejected from a volcanic vent. Pyroclastic particles (pyroclasts) form by disintegration of magma as gases are released by decompression and then ejected from a volcanic vent. Pyroclastic ejecta can be categorized according to origin, i.e.

Essential (or juvenile) These are pyroclasts derived directly from erupting magma and consist of dense or inflated particles of chilled melt, or crystals (phenocrysts) in the magma prior to eruption.

Cognate (or accessory) Cognate particles are fragmented comagmatic volcanic rocks from previous eruptions of the same volcano.

Accidental Accidental fragments (or "lithoclasts") are derived from the sub-volcanic basement rocks and therefore may be of any composition.

Alternatively, pyroclasts can be sorted according to grain size, where ash is defined to be composed of particles < 2 mm in diameter. Volcanic ash is composed of vitric, crystal or lithic particles (of juvenile, cognate or accidental origin) of various proportions. Larger fragments, lapilli (2 - 64 mm) or bombs (> 64 mm) follow ballistic trajectories and are not contained within the mature eruption cloud.

1.3 Volcanic Ash Properties

Composition The physical properties of volcanic ashes depend mostly on their relative proportions of glass, mineral fragments and rock fragments. Table 3 from Heiken (1994) summarizes the properties of volcanic ash as a function of eruption type. The physical properties of ash particles are principally determined by the chemical composition of these components and their grain size. Gooding et al. (1983) obtained ash samples from the 1983 El Chichón volcanic ash cloud and used x-ray spectrometry to conclude that the ash particles were predominately vesicular glass shards of rhyolitic-andesitic bulk composition.

Eruption Type	Ash Composition			Types of glass particles in ash
	Glass shards and Pumice	Mineral Grains	Rock Fragments	
Hawaiian	60-80	1-5	20-40	cm to mm angular droplets and bombs
Stombolian	60-80	1-5	20-40	cm to mm angular blocky fragments
Vulcanian	10-30	10-30	70-90	mm angular fragments and rare drops
Plinian	60-100	0-35	0-30	cm to μm angular shards and pumice
Plinian-hydrovolcanic	60-100	0-35	0-40	mm to μm angular shards and rare pumice

Table 3: Properties of volcanic ash as a function of eruption type

Bayhurst et al. (1994) give the density of ash from the December 15 eruption of Mt Redoubt as 2.42 ± 0.79 g cm^{-3}.[1] In addition they found the average aspect ratio and surface area of an ash particle to be 3.5 and 284 μm^2 respectively.

Volcanic ash is abrasive, mildly corrosive and conductive (especially when wet) and may also carry a high static charge. The melting properties of volcanic ash typical of circum-Pacific volcanoes have been investigated

[1] Thus a value of ash loading in mg m^{-3} $\times$ 413 is approximately the particle volume density in μm cm^{-3}.

by Swanson and Beget (1994). They found the melting temperature of the rhyolitic (silica-rich) glasses ranged from 1000°C to 1300°C whereas the minerals (feldspars, pyroxene, hornblende and Fe-Ti oxides) begin melting at about 1100°C.

Size Distribution The initial particle size distribution of tephra is poorly understood although Sparks et al. (1994) note that 70 % of ejecta from explosive eruptions is less than 1 mm in radius. Hobbs et al. (1991) measured the in situ particle size distributions from ash emissions by Mt Redoubt, Mt St Helens and Mt St Augustine. The size distributions were approximately multimode lognormal distributions with a nucleation mode ($r_{mode} < .05$ μm) an accumulation mode ($r_{mode} \approx .05$ μm $- 0.5$ μm) and one or more giant modes ($r_{mode} > 0.5$ μm). Hobbs et al. considered the nucleation mode to be composed of sulphuric acid – water drops where the H_2SO_4 was produced either in the volcanic throat or by gas to particle conversion of the SO_2 in the eruption plume. The accumulation and giant modes were thought to be composed of silicate particles.

Hobbs et al. made two in situ measurements of the volcanic ash cloud following the 15 minute eruption of the Redoubt Volcano on 8 January 1990. The particle size spectrum 2 1/2 hours after the eruption contained mostly accumulation mode particles, while the spectrum measured 7 hours after the eruption contained predominantly nucleation mode particles. However in both measurements most of the particle mass was contained in giant particles (radius ≈ 5 μm – 50 μm) so that maxima in particle volume as a function of radius size occur at radii of 5 and 15 μm.

Radius (μm)	**Fall Speed (m s^{-1})**	**Residence Time**
700	9	9.3 min
355	6.4	13.0 min
173	3.2	26.0 min
85	1.9	43.0 min
45	0.64	2.2 hrs
22	0.15	9.3 hrs
11	0.05	1.1 days
5.5	0.012	4.8 days
2.75	0.0025	23.1 days

Table 4: Estimated particle terminal velocities and residence times.

The evolution of the ash cloud was principally a decrease in the concentration at all particle sizes. This is not surprising as the residence time of a volcanic ash particle is strongly controlled by its mass (i.e. size) and non-spherical morphology (Mackinnon et al., 1984). Table 4 from Bursik et al. (1994) shows the estimated terminal velocity and typical residence times as a function of particle size for an ash cloud with a particle density of 2 g cm^{-3} at 12.9 km. Some of the smaller particles aggregate into clusters due to electrostatic attraction giving them settling velocities higher than those shown i.e. $\approx 0.3 - 1.0$ m s^{-1} (Macedonio et al., 1994).

A fit of the initial Mt Redoubt ash size distribution derived from measurements by Hobbs et al. (1991) is shown in the top panel of Figure 2. This distribution is consistent with the conclusion of Knollenberg and Huffman (1983) that volcanic material injected into the stratosphere by large volcanic eruptions is typically less than 1 μm in radius. It is important to realise that most of the ash mass in the early lifetime of a cloud is contained in relatively large particles (see lower panel of Figure 2) i.e. 90 % of the mass of the volcanic cloud is contained in particles bigger than 2 μm. Also shown in Figure 2 is the size distribution for the 2 day old Mt St Helens volcanic cloud derived from measurements at 17 km by Farlow et al. (1981).

Calculations by Sparks et al. (1994) gave the mass loadings of the umbrella part of a volcanic clouds as varying from 2500 to over 20000 mg m^{-3} for columns from 7 to 40 km. The US military regard particle loadings of 50 mg m^{-3} or more as potentially hazardous. The fresh and aged size distributions shown in Figure 2 have

total particle volumes of 20640 μm cm^{-3} (i.e. $\approx$ 50 mg m^{-3}) and 3.9 μm cm^{-3} (i.e. $\approx 9.4 \times 10^{-2}$ mg m^{-3}) respectively.

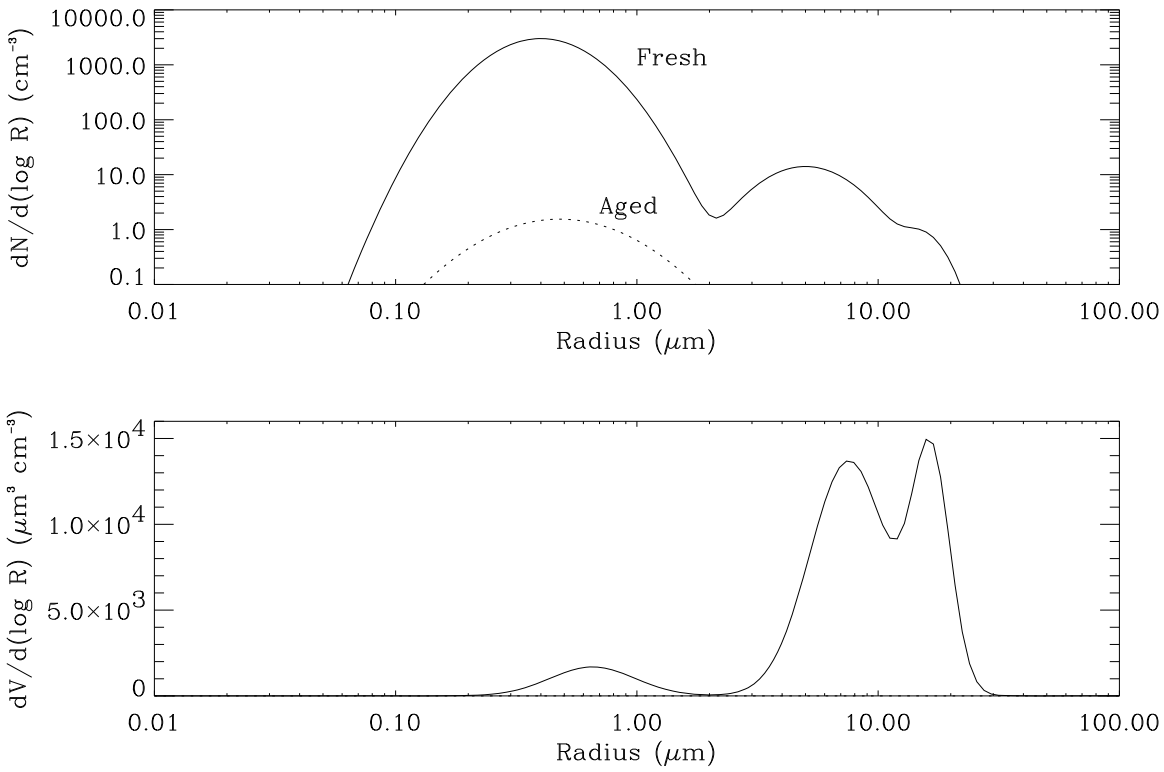

Figure 2: Trimodal log-normal particle size distribution representative of a young ($\approx$ 2 1/2 hrs after eruption) volcanic ash cloud (N_1 = 3056 cm^{-3}, r_1 = 0.4 μm, σ_1 = 1.5, N_2 = 13.1 cm^{-3}, r_2 = 5 μm, σ_2 = 1.45, N_3 = 0.375 cm^{-3}, r_3 = 15 μm, σ_3 = 1.2). Also shown is a monomodal lognormal particle size distribution representative of an aged ($\approx$ 2 days after eruption) ash cloud (N = 2.15 cm^{-3}, r = 0.478 μm, σ = 1.74).

Optical Properties The most comprehensive measurements of the optical properties of volcanic ash to date are those of Volz (1973). He measured the spectral transmission for:

- ashfall from an eruption of Irazú, Costa Rica which was composed of 0.05 mm to 0.5 mm shards of a dark grey ash with feldspar,
- an ash sample from Kilauea, Hawaii composed of slightly weathered vesicular glass similar to perlite,
- fly-ash from the electrostatic cleaning chamber of a power plant fired with powdered coal. These particles were spherical with a mode radius of 0.3 μm.

The transmission spectra of all these samples was similar to spectra of greenish light-weight pumice. Using the optical constants of Volz it is possible to estimate the infrared extinction spectra typical of fresh and aged volcanic clouds (Figure 3). If the fresh ash concentrations were increased to the levels suggested by Sparks et al. (1994) then the extinction would be even higher. The reduction in the volume of ash as a cloud ages is reflected in the reduction in the infrared extinction by about three orders of magnitude. In addition the fresh cloud shows very little spectral variation. This is due to the large number of giant particles which act as efficient scatterers of the relatively short wavelength infrared radiation. These particles are not present in the aged cloud so the extinction spectrum then shows structure typical of an absorption spectrum. In addition Figure 3 shows

extinction spectra for water ice (cirrus cloud) and for sulphuric acid (background aerosol haze). Ash is clearly distinguishable from the background sulphuric acid loading on the magnitude of the extinction alone. The ash and ice clouds are separable in terms of their spectral features, ice having an absorption feature at about 10 μm and ash having a similar feature at about 8 μm.

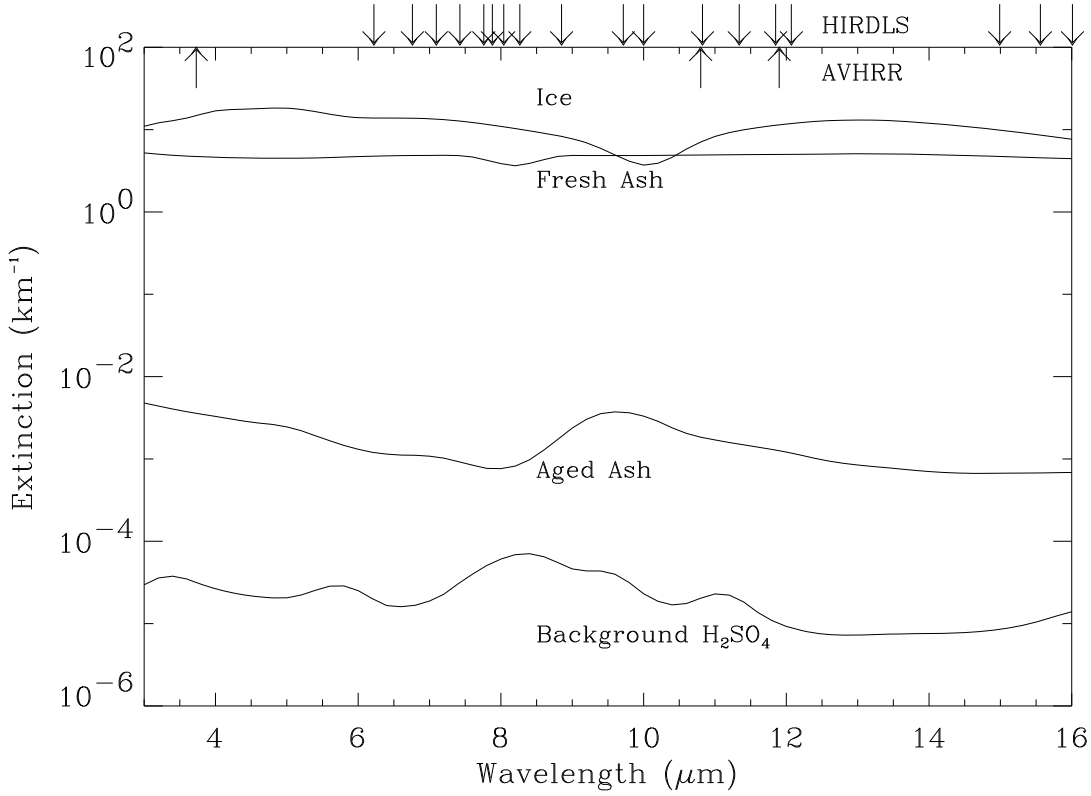

Figure 3: Extinction spectra calculated for: the fresh and aged volcanic ash size distributions shown in Figure 2 using the refractive indices of Volz (1973); a cirrus type particle size distribution (Deirmendjian, 1969) using the refractive indices of Toon et al. (1994); a background sulphuric acid aerosol size distribution (Grainger, 1993) using the refractive indices typical of 75 % sulphuric acid from Palmer and Williams (1975). Arrows along the top axis show the central wavelength of two remote sensing instruments discussed in Section 3.

It should be noted that these calculations assume that the particles are spherical and are of a single composition, which is reasonable in a first order calculation. In addition, for optically thick cloud multiple scattering can occur, which will result in a reduction of the spectral features. In reality the aged volcanic ash may be coated with a layer of sulphuric acid and it is likely that the extinction spectra will contain a contribution from the nucleation mode sulphuric acid particles. Another complication is the coating of ash particles with water ice, particularly for a hydrovolcanic eruption.

2 Aircraft Encounters with Volcanic Plumes

2.1 Frequency of Encounter

Worldwide, more than 1,500 volcanoes have erupted in the last 10,000 years, and about 630 of these have erupted in historical time (Simkin and Siebert, 1994). On average, about 60 volcanoes erupt each year, of which about 10 inject material to aircraft cruising altitudes (Self and Walker, 1994). Appendix 3.4 provides a non-exhaustive list of aircraft-ash encounters that have appeared in the scientific literature. Casadevall (1994) state that between 1980 and 1994 eighty jet airplanes have been damaged by unplanned encounters with drifting clouds of volcanic ash in air routes and at airports. It is expected that this average rate of 5.3 encounters per year is increasing with increased air traffic, however the natural variability of volcanism implies that there will be high year-to-year variability about the trend.

The possibility of aircraft ash encounters is especially high throughout the North Pacific (NOPAC) region. Volcanic ash is estimated to invade north pacific air routes four days per year. These routes are used by about 70 flights a day carrying about 10,000 passengers. About one hundred active volcanoes lie close to the NOPAC air corridor and are located in three regions:

Kurile Islands Eruptions from the 30 volcanoes lying within 220 km of the west end of the NOPAC air routes are a particular danger to west-bound traffic which, if low on fuel, may have limited ability to manoeuvre around ash clouds.

Kamchatka Peninsula International air routes lie both off-shore and directly over 30 active volcanoes that extend along this 740 km peninsula.

Alaska NOPAC air routes lie off-shore of over 40 active volcanoes along the 2,600 km of the Alaskan Peninsula and Aleutian islands.

2.2 Effect of Volcanic Ash on Aircraft

The primary effect of volcanic ash on aircraft is caused by the ash melting and adhering to engine parts. In particular the adherence of melted and resolidified ash can reduce the effective flow of air through the engine . Dunn and Wade (1994) noted that several different mechanisms may be responsible for altering engine performance during an encounter with a volcanic cloud including:

- deposition of material on hot-section components,
- erosion of compressor blades and rotor path components,
- partial or complete blockage of fuel nozzles,
- partial or total blockage of cooling passages,
- oil system or bleed air supply contamination,

in addition the aircraft can experience:

- fogging of the windscreen and landing lights,
- ash contamination of electronics causing arcing and short circuits,
- erosion of antenna surfaces,
- plugging of the pitot-static system (airspeed indication),
- exposure of crew and passengers to toxic fumes, and ash particles.

The increase in engine failures from ash ingestion since 1982 is because jet engines run at higher temperatures than older aircraft. Modern engine temperatures are typically 1000 to 1200 °C (cf. ash melting point of about 800 °C). At cruising altitudes, 150 tons of air per minute passes through each of the four engines of a Boeing 747. Thus even if the ash is barely detectable to the naked eye substantial amounts of ash can be ingested into the engines.

2.3 Hazard Avoidance

2.3.1 In Flight Recognition

Harris and Rose (1983) observed that ash clouds which are a hazard to aircraft (densities of 0.08 - 3.4 g m^{-3}) have radar reflectivity several orders of magnitude smaller than the reflectivity for severe weather so do not appear on on-board radar. Visual recognition of a volcanic hazard may be difficult at night or during the day as ash clouds commonly look like normal weather clouds. Campbell (1994) provides the following list of conditions that may be indicative of volcanic ash:

- static discharge (St Elmo's fire) around the windshield accompanied by a bright white glow in the engine inlets,
- at night, landing lights cast sharp distinct shadows (unlike the fuzzy, indistinct shadows that are cast against weather clouds),
- volcanic ash (haze) appearing in the cockpit and cabin,
- an acrid odour similar to electrical smoke or burnt dust. The smell of sulphur may also be present,
- decrease in airspeed,
- loss of cabin pressure,
- multiple engine malfunction.

2.3.2 International

The International Civil Aviation Organization (ICAO) has set up a network of Volcanic Ash Alert Centres (VAACs), to provide forecasts of ash cloud dispersion to the civil aviation industry (see Table 2.3.2). Information on increasing volcanic activity, a volcanic eruption or a volcanic ash cloud is passed to the VAAC from primary observing sources (including domestic/international aviation, volcanological, seismological, geological, meteorological) or other (e.g. police, military) networks.

Volcanic ash advisory centre	Areas of Responsibility
Anchorage (United States)	Anchorage Oceanic, Anchorage Continental, Anchorage Arctic
Buenos Aires (Argentina)	South of 10°S between 30°W and 90°W
Darwin (Australia)	Southward from 10°N and from 100°E to 160°E
London (United Kingdom)	Bødo Oceanic, Reykjavik, Shanwick Oceanic, London, Scottish Shannon
Montreal (Canada)	Søndrestrøm, Gander Oceanic, Canadian Continental flight information regions (FIRs) including the Arctic Ocean
Tokyo (Japan)	60°N to 10°N and from 100°E to Oakland Oceanic and Anchorage Oceanic and Continental FIR boundaries
Toulouse (France)	Santa Maria Oceanic, AFI Region, EUR (except for London, Scottish and Shannon FIRs) and MID Region south of 71 °west of 60°E
Washington (United States)	New York Oceanic, Oakland Oceanic, and United States Continental FIRs, CAR Region, SAM Region, north of 10°S
Wellington (New Zealand)	Equator to 60°S and 160°E to 140°W

Table 5: Volcanic ash advisory centres designated by ICAO.

The VAACs parallel the Regional Specialized Meteorological Centres (RSMCs) in concept, and in most examples national RSMCs and VAACs are coincident. An international SIGnificant METeorlogical Information (SIGMET) bulletin advises of weather potentially hazardous to all aircraft. The purpose of this information is to advise pilots of the occurrence or expected occurrence of en-route weather phenomena which may affect the safety of aircraft operations.

3 Observing Volcanic Ash Clouds Using Satellite Instruments

This section considers whether satellite instruments in general and the High Resolution Dynamic Sounder (HIRDLS) in particular can recognize volcanic ash clouds. Two scenarios are considered:

1. the recognition of a fresh ash cloud within 2 – 6 hours of eruption.
2. the monitoring of an existing ash cloud to provide flight path hazard proximity assessment.

3.1 Satellite Instrumentation

There are many existing and proposed multi-spectral satellite instruments that observe the Earth's atmosphere using wavelengths roughly between about 0.3 μm to about 16 μm. These instruments can be subdivided into two categories:

Surface Remote Sensing Instruments: Data from surface remote sensing instruments (e.g. the Advanced Spaceborne Thermal Emission and Reflection Radiometer (ASTER) on the EOS AM-1 satellite) is generally very high resolution ($<$ 100 m) and it takes several weeks to achieve global coverage (revisit the same scene). Generally, data processing algorithms for these instruments are developed to interpret the surface signal by correcting for any atmospheric signal (e.g. water vapour absorption) or ignoring 'contaminated' pixels (e.g. cloud). Although it may be possible to include these type of instruments in a volcanic ash warning system, because of their extremely low spatial coverage they are omitted from any further discussion.

Meteorological Instruments: Operational and proposed meteorological instruments are further categorized and listed in Table 6. Description of these instruments are provided in Appendix B. Instruments with extremely limited spatial coverage have been excluded from this list, e.g the solar occultation instruments: the Stratospheric Aerosol And Gas Experiment (SAGE) II and the Halogen Occultation Experiment (HALOE) which typically observe about 24 locations per day.

Several of the instruments (e.g. TOMS, AVHRR) are part of long term programmes which involve the operation of similar instruments on several platforms. Generally the nadir observing instruments provide global data at a relative high frequency ($>$ once per day) and moderate spatial resolution (roughly 1 km^2). The main disadvantage of these instruments is their lack of vertical resolution so that the measurement of the height of a volcanic plume and the separation of volcanic ash from water/ice clouds is not necessarily achievable.

The advantage of limb viewing instruments is their ability to vertically resolve the atmosphere, in particular to geometrically discriminate a volcanic plume above cloud. Limb viewing is most effective in the stratosphere; in the troposphere the long observation path makes the measurement susceptible to cloud contamination. Solar occultation instruments observe approximately 24 sunrise/sunsets a day giving them extremely poor spatial coverage. This problem can be somewhat mitigated by including lunar and stellar occultations.

Geostationary

Multispectral Imaging Radiometer (MIR)
Very High Resolution Radiometer (VHRR)
Scanning Television Radiometer (STR)
GOES I-M Imager
Visible Infrared Spin-Scan Radiometer (VISSR)

Low Earth Orbit

Nadir Viewing Instruments
Advanced Very High Resolution Radiometer (AVHRR)
Along Track Scanning Radiometer (ATSR)
Global Ozone Monitoring Experiment (GOME)
Moderate-resolution Imaging Spectroradiometer (MODIS)
Operational Linescan System (OLS)
Total Ozone Mapping Spectrometer (TOMS)

Limb Viewing Instruments (Occultation)
Global Ozone Monitoring By Occultations Of Stars (GOMOS)
Stratospheric Aerosol And Gas Experiment (SAGE) III

Limb Viewing Instruments (Atmospheric Emission)
High Resolution Dynamics Limb Sounder (HIRDLS)
Michelson Interferometer for Passive Atmospheric Sounding (MIPAS)

Nadir and Limb Viewing Instruments
Scanning Imaging Absorption Spectrometer For Atmospheric Chartography (SCIAMACHY)

Table 6: Operational and planned meteorological instruments.

3.2 Current Multispectral Techniques

Volcanic Ash Observations Prata (1989) demonstrated that it was possible to discriminate idealised volcanic ash clouds from water and ice clouds using AVHRR Channels 4 and 5. The temperature difference (T4 - T5) between these two channels is negative when observing small volcanic ash particles (≈ 1 μm) but is positive for surface and most water clouds. This method was used by Holasek and Rose (1991) to analyse the 1986 eruptions of the Augustine volcano, Alaska and by Wen and Rose (1994) to investigate the 19 August 1992 eruption of Crater Peak/Spurr Volcano Alaska. However there are limits on the applicability of this approach:

- Hydrovolcanic eruptions can lead to volcanic clouds containing large amounts of ice whose spectral signature is opposite to that from the ash particles. Rose et al. (1995) demonstrate this effect for the 19 September 1994 eruption of Mt Rabaul, Papua New Guinea.
- The large particles present in the volcanic cloud for the few days following an eruption result in the cloud acting as both an efficient emitter and scatterer of infrared radiation. Consequently the temperature difference between channels 4 and 5 is difficult to interpret and can be positive so giving the cloud the same signature as a water or ice cloud.

The shortwave AVHRR channels are highly dependent on cloud optical thickness although Kerdiles and Diaz (1996) were able to map the settled ash following the eruption of Cerro Hudson in 1991. One interesting possibility would be the incorporation of AVHRR channel 3 data which has been shown to contain cloud particle size information (Grainger, 1990). Harris et al. (1995) demonstrated that it was possible to detect a

major thermal anomaly in AVHRR Channels 3, 4 and 5 during the eruption of Krafla, Iceland during September 1984. Thus monitoring the surface for temperature anomalies may provide pre-eruption warning. However a detailed analysis of this approach is outside the scope of this report.

3.3 Using HIRDLS to warn aircraft of collision with volcanic ash clouds

The HIRDLS observation 'footprint' for an atmosphere measurement is approximately a box 1 km thick, 224 km along the line-of-sight and 10 km wide centred on the tangent point. Figure 4 shows the HIRDLS scan pattern for one day represented by ± 112 km vectors centred on the tangent point along the line-of-sight. Although global coverage is obtained within 12 hours, the sampling of all atmospheric locations takes several days.

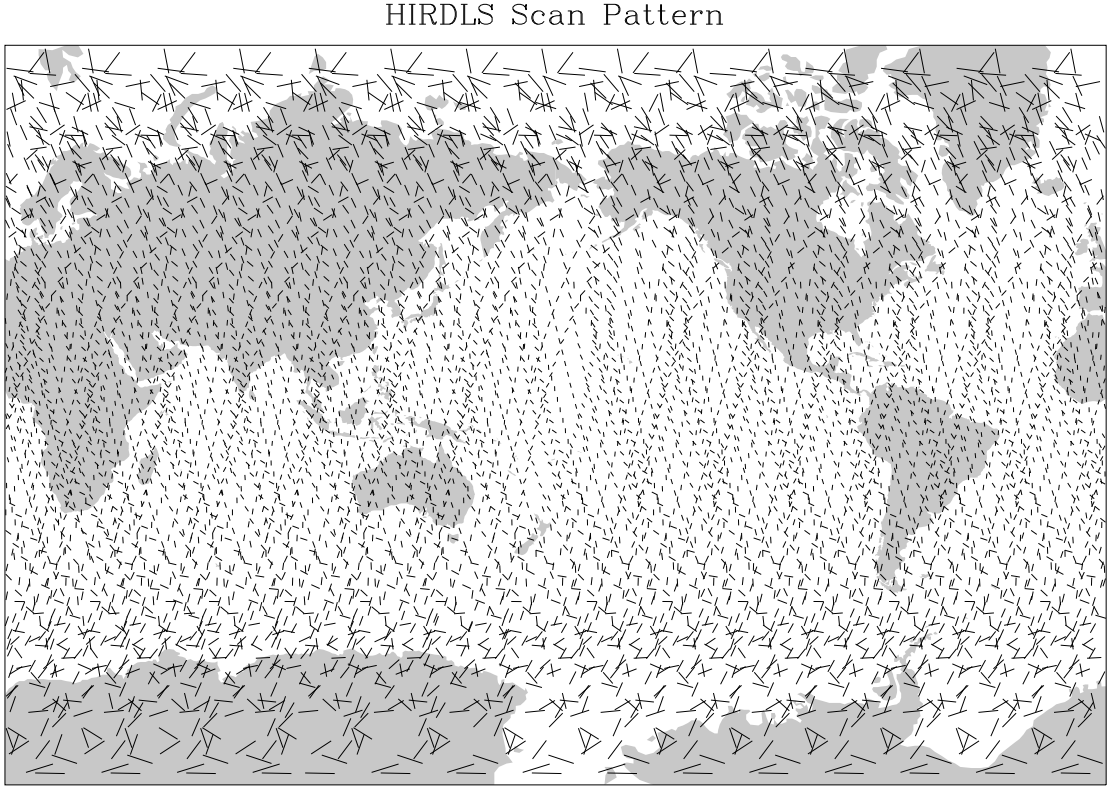

Figure 4: Line-of-sight vectors centered on the HIRDLS tangent point for a typical 1 day observation sequence.

As discussed in Section 1 volcanic plumes grow rapidly during and following an eruption. The probability of HIRDLS observing a volcanic plume is critically sensitive to the plume size. If one assumes a plume radii of 50 km centred on the USGS Holocence volcano locations then on average HIRDLS 'observes' about 18 locations per hour. For a 275 km plume radius typical of a 2 hours post-eruption plume the observation rate is about 70 locations per hour. These numbers represent 1 % and 5 % of the known volcanoes respectively. Figure 5 shows that it takes 2 days for HIRDLS to observe 40 % of known volcano locations given a plume radius of 50 km. A similar fraction of volcanic locations is observed in about 8 hours if a plume radius of 275 km is chosen.

Figure 5 does indicate that HIRDLS would observe a large volcanic ash cloud several times during its lifetime (typically up to a week) so it would be possible to monitor the evolution of a cloud. HIRDLS can distinguish an ash cloud from an ice or water cloud geometrically although its particular advantage is the large number of infrared channels (see Figure 3 or Appendix B.4). This location of the channels will provide the ability to determine if a cloud is ice or ash or a mixture of the two on a point by point basis.

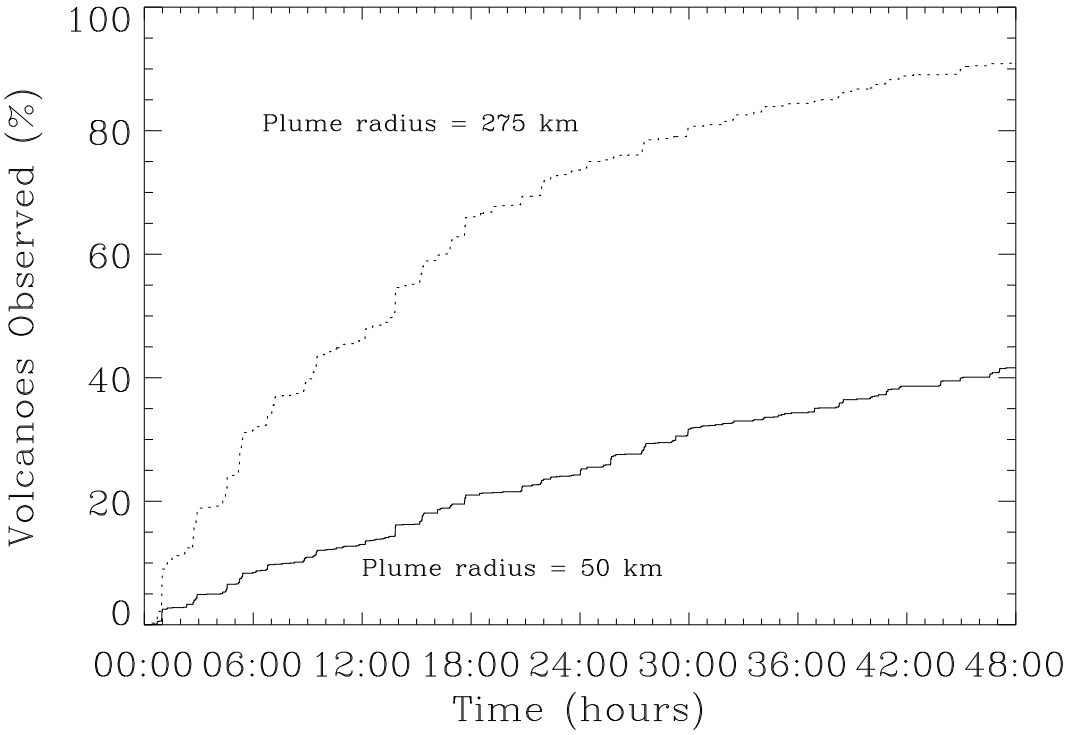

Figure 5: Percentage of active volcano locations observed as a function of time assuming either a 50 km or 275 km plume radius.

3.4 Conclusions

The main conclusions are

i) There are concerns about HIRDLS pixel size, and to what extent ash clouds would fall between pixels; this would effectively reduce the sampling interval for a given location from 12 hours to perhaps 24, 36 or 48 hours. Nevertheless HIRDLS could provide flight path hazard proximity warnings for a long-lived moderate to large ash cloud.

ii) Study of the spectral properties shows that very young ash (<12 hours) may have a particle size distribution that makes discrimination from meteorological clouds more difficult than previously thought. This should have a more serious effect on vertical imager 'two-colour' techniques than on HIRDLS data, since the latter benefits also from using geometry to identify stratospheric ash. Hence on balance, this makes the HIRDLS data more useful than previously thought for the stratosphere, but in the troposphere, it means that both limb and vertical view data are less useful (and probably explains past problems with vertical view data).

iii) Ash warnings based on HIRDLS data would be most effectively distributed through the standard ICAO warning system.

iv) Joint retrieval of HIRDLS data with those from other satellite sensors is not viable, and any combined use of data would have to be performed at high level by human effort.

Acknowledgements

Grateful thanks are expressed to T. Fox of the ICAO for providing the operational procedures used by ICAO to warn of volcanic ash contamination of airways. Anu Dudhia kindly provided the MIPAS scan pattern. This report was funded by a NERC Connect-A award.

A Documented Aircraft – Ash Encounters

Date	Air Route	Altitude	Aircraft	Impairment and Damage	Reference
			Irazú, Costa Rica		
1963			Pan Am DC-6	Abrasion of windows and engines, forced landing in Panama	Barquero (1994)
			Augustine Volcano, Alaska		
22 January 1976	Galena - King Salmon	31,000 ft	F-4E	limited visibility, abrasion damage to canopy	Harris and Rose (1983)
25 January 1976	Anchorage - Tokyo	33,000 ft	Japan Airlines DC-8 (JAL 672)	Ash adhered to the plane and abrasion to external radio parts, landing gear and air-conditioning system	Kienle (1994)
25 January 1976	Anchorage - Tokyo		Japan Airlines 747	minor damage	Kienle (1994)
25 January 1976	Anchorage - Tokyo		Japan Airlines DC-8	minor damage	Kienle (1994)
			Mt St Helens, Washington		
18 May 1980	San Francisco - Calgary	35,000 ft	DC 9	damaged compressor blades; damaged windscreen; exposure 4 minutes	Harris and Rose (1983)
25 May 1980	Tacoma - Sacramento		Transamerica L100 (C-130)	functional loss of two engines; impaired emergency landing; damage and replacement of four engines	Harris and Rose (1983)
26 May 1980			DC 9	seizure of first-stage midspan shrouds in all engines	Harris and Rose (1983)
			Mt Galunggung, Indonesia		
5 April 1982	Jakarta - Yogjakarta		Garuda Airlines DC-9	aircraft required maintenance	Johnson and Casadevall (1994)
24 June 1982	Kuala Lumper - Perth	37,000 ft	British Airways 747-200 (BA 009)	temporary loss of four engines; descent to 12,500 ft while attempting engine restart; abrasion of windscreen; emergency landing on three engines	Harris and Rose (1983)
24 June 1982	Kuala Lumper - Perth		Singapore Airlines 747 (SQ 24A)	'smoke' contaminated the main cabin, small fragments of rock were found in all engine tailpipes	Johnson and Casadevall (1994)
12 July 1982	Singapore - Melbourne	33,000 ft	Singapore Airlines 747-200 (SQ 21A)	functional loss of two engines; emergency landing on remaining two engines	Harris and Rose (1983)

Table 7: A non-exhaustive list of significant ash encounters by commercial aircraft. Many non-specific estimates are also available, e.g. Casadevall (1994) states that between 1980 and 1994 80 jet airplanes have been damaged by unplanned encounters with drifting clouds of volcanic ash in air routes and at airports. Seven of these encounters caused in-flight loss of jet engine power.

Date	Air Route	Altitude	Aircraft	Impairment and Damage	Reference
			Colo Volcano, Una Una Island, Sulawesi		
23 July 1983	Singapore - Perth	35,000 ft	British Airways 747	returned to Singapore, no significant damage	Johnson and Casadevall (1994)
			Soputan Volcano, Sulawesi		
19 May 1985	Hong Kong - Melbourne		Quantas Airways 747 (QF 28)	cabin filled with dust, aircraft engines had to be removed and cleaned	Johnson and Casadevall (1994)
			Redoubt Volcano, Alaska		
14 December 1989	Amsterdam - Anchorage		KLM 747-400 (KLM 867)	Flame out of all four engines; major aircraft damage	Przedpelski and Casadevall (1994)

Table 7: Continued

B Satellite Instruments

B.1 Geostationary

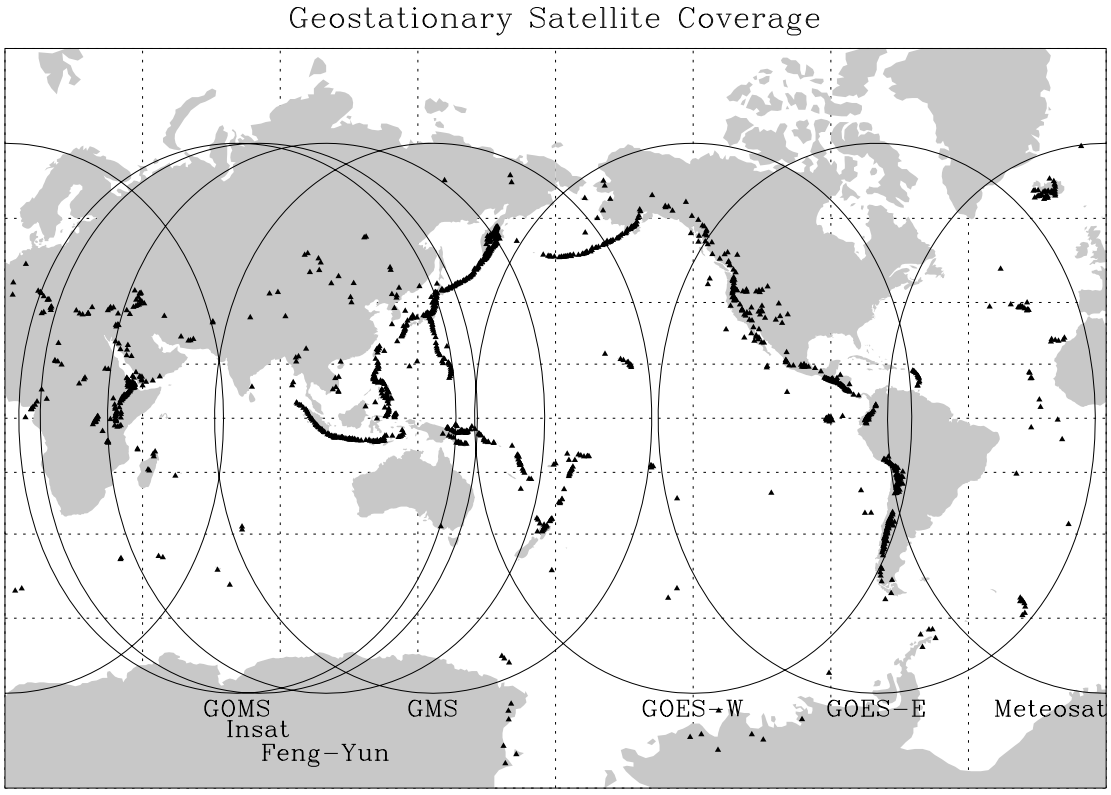

Figure 6: Geostationary satellite locations and coverage. The coverage extremes are chosen to be those locations where a geostationary satellite is 10° above the horizon. Also shown are the Holocene volcano locations.

Geo-stationary satellites orbit about 35,798 km above the Earth. Their motion is synchronized with the Earth's rotation so that they remain stationary over a point above the Earth's equator (satellite subpoint). The spatial coverage of the 8 operational geostationary meteorological satellites is shown in Figure 6. Each satellite observes about 25 % of the Earth's surface, generally 50° of latitude North and South of the equator and 50° of longitude East and West of the satellite's position along the equator (subpoint). Of the 1509 volcanoes listed by the USGS all but 14 are observed by one or more geostationary satellites (see Table 8).

Name	Launch Date	Location	Volcanoes Observed
Meteosat-6	20 November 1993	0.5° E	383
GOMS	31 October 1994	76° E	576
Insat-2B	22 Jul 1993	83° E	646
Feng-Yun	10 June 1997	105° E	720
GMS-5	17 Mar 1995	140° E	711
GOES W (9/J)	23 May 1995	135° W	587
GOES E (8/I)	13 April 1994	75° W	458

Table 8: Operation geostationary satellites.

The following list summarises the sensors carried on the geostationary platforms, the ingest (data process-

ing) time and the data availability.

Meteosat (Europe), currently operational: Meteosat-6.

Imaging Radiometer: The Multispectral Imaging Radiometer (MIR) provides full Earth images every 30 minutes in one visible (0.4 - 1.1 μm) and two infrared channels (5.7 – 7.1 μm, 10.5 – 12.5 μm). The sub-satellite resolution is 2.5 km in the visible band and 5.0 km in infrared bands.

Ingest: The raw (uncorrected) images are received by EUMETSAT in Darmstadt. After they have been rectified (geometrically corrected), they are re-disseminated via Meteosat to the user community according to a fixed schedule. Image data are sent as WEFAX formats and High Resolution Information (HRI). All high resolution image data, except for 00, 06, 12 and 18 UTC are subject to image encryption.

Future: Meteosat Second Generation (MSG) (aka Meteosat II) is a 12-channel spinning Imager now under construction. MSG will be capable of full-disk images every 15 minutes, although it may not be able to downlink all of that data at full resolution. MSG is expected to launch in the year 2000.

GOMS (aka ELEKTRO or ELECTRO) (Russia), currently operational: GOMS-1.

Imaging Radiometer: GOMS is Russia's first geosynchronous weather imaging satellite and carries the Scanning Television Radiometer (STR). The STR is a two-channel device, sensing in the visible (0.46 – .7 μm) and infrared (10.5 – 12.5 μm). The sub-satellite resolution is 1.25 km in the visible and 6.l25 km in the infrared. Sensor problems restrict the availability of visible images.

Ingest: Real time image data is supposedly available through the internet at http://smis.iki.rssi.ru/goms/-goms_d.htm, but in practice the latest online images are two months old.

INSAT (India), currently operational: Insat-2B.

Imaging Radiometer: The INSAT carries a Very High Resolution Radiometer (VHRR) operating in the visible (0.55 – 0.75 μm) and infrared (10.5 – 12.5 μm) regions. The spatial resolution in the visible is 2 km and in the infrared 8 km. The radiometer takes about 23 minutes to view the Earth's full disc. Sector scans are possible. Normally images are taken once in three hours. Currently both visible and infrared images are available from 83° East orbital position but only visible images are available from from 93.5° position.

Ingest: INSAT imagery is reportedly encrypted to hide it from the surrounding nations. Apparently NOAA has been negotiating for years to get regular access to realtime INSAT imagery. There are supposedly no problems with archived imagery, only real time data is an issue. The INSAT images are currently not available over the internet.

Future: INSAT-2E to be launched in the first half of 1998 to the 83° position will incorporate a VHRR which has an additional water vapour channel (5.7-7.1 microns) with 8 km resolution. A charge Coupled Device (CCD) camera in the visible (0.63 – 0.69 μm), near infrared (0.77 – 0.86 μm) and short wave infrared (1.55 – 1.70 μm) bands with 1 km resolution will also be added.

Feng-Yun (China), soon to be operational: Feng-Yun-2.

Imaging Radiometer: Feng-Yun-2 is China's geostationary meteorological satellite, a copy of the GMS-5 satellite and as such carries the Visible Infrared Spin-Scan Radiometer (VISSR).

Ingest: Direct broadcast of the FY-2 data will begin in October 1997 and will be collected by a ground station at the University of Southern Australia in Adelaide for distribution over the internet.

GMS (Japan), currently operational: GMS-5.

Imaging Radiometer: The Visible Infrared Spin-Scan Radiometer (VISSR) provides full Earth images every 30 minutes in one visible (0.5 - 0.75 μm) and three infrared channels (6.5 – 7.00 μm, 11.2 – 12.2 μm, 11.5 – 12.5 μm). The sub-satellite resolution is 2.5 km in the visible band and 5.0 km in infrared bands.

Ingest: GMS data is available over the internet in near real-time from http://rsd.gsfc.nasa.gov/goesg/-earth/Weather/GMS-5/

GOES (USA), currently operational: GOES W (9/J) and GOES E (8/I).

Imaging Radiometer: The GOES-I/M Imager is a multi-channel nadir viewing instrument series similar to the AVHRR (see Table 9).

Channel	Wavelengths (μm)	Nadir E-W $\times$ N-S Resolution (km)
1	0.55 – 0.75	0.57 $\times$ 1
2	3.8 – 4.0	2.3 $\times$ 4
3	6.5 – 7.00 (I/J/K/L)	2.3 $\times$ 8
	13.0 –13.7 (M)	
4	11.2 – 12.2	2.3 $\times$ 4
5	11.5 – 12.5 (I/J/K/L)	2.3 $\times$ 4
	5.8 – 7.3 (M)	

Table 9: GOES-I/M spectral channels.

The field of view of adjacent Imager pixels overlaps so that complete coverage is provided in a full-Earth disc image which takes about about 25 minutes to acquire. However the Imagers on both GOES-E and GOES-W follow a complicated scanning schedule. For example the routine schedule for GOES-E is for 6 frames per hour: 2 for conterminous United States (xx00 and xx30 UTC); 2 for the 'roaring 40's' around South America (xx10 and xx40 UTC); 2 for Canada-to-Brazil (xx015 and xx45 UTC). There are 8 Full-Earth scans per day, occurring once every 3 hours, at 0245, 0545, 0845, 1145, 1445, 1745, 2045, and 2345 UTC. Similarly GOES-W obtains a full disk image once every three hours.

Ingest: Raw data is calibrated, geographically registered and reformatted in near real time at NASA GSFC and immediately made available though the internet (GOES-8, http://rsd.gsfc.nasa.gov/-goese/autogvar/goes8/; GOES-9, http://rsd.gsfc.nasa.gov/goesf/autogvar/goes9/).

Future: The National Oceanic and Atmospheric Administration is in the process of procuring new geostationary operational satellites to replace the current series of satellites, which will reach the end of their useful lives around 2002.

In summary geostationary satellites provide observations of nearly all volcanic locations once every three hours or better in two to five spectral channels.

B.2 Low Earth Orbit: Nadir Viewing Instruments

B.2.1 Advanced Very High Resolution Radiometer (AVHRR)

Instrument Description The Advanced Very High Resolution Radiometer (AVHRR) is a broad-band, four or five channel scanner (depends on model, see Table 10), sensing in the visible, near-infrared, and thermal infrared portions of the electromagnetic spectrum (Kidwell, 1995). The AVHRR sensor is carried on NOAA's Polar Orbiting Environmental Satellites (POES), beginning with TIROS-N in 1978 (see Table 11). The POES are a series of satellites in 870 km (nominal) circular, near-polar, sun-synchronous orbits with an inclination angle of approximately 99 degrees (retrograde) to the equator. They cross the equator during local morning

and afternoon (and corresponding night-times), with an orbital period of approximately 102 minutes. Each sequential orbit covers adjacent longitudes near the equator and overlapping longitudes near the poles.

Band	Satellites: NOAA-6, 8, 10	Satellites: NOAA-7, 9, 11, 12, 14	IFOV (milliradians)
1	0.58 μm – 0.68 μm	0.58 μm – 0.68 μm	1.39
2	0.725 μm – 1.10 μm	0.725 μm – 1.10 μm	1.41
3	3.55 μm – 3.93 μm	3.55 μm – 3.93 μm	1.51
4	10.50 μm – 11.50 μm	10.3 μm – 11.3 μm	1.41
5	band 4 repeated	11.5 μm – 12.5 μm	1.30

Table 10: AVHRR Spectral Bands

Satellite Number [a]	Launch Date	Ascending Node [b]	Descending Node	Service Dates
TIROS-N	10/13/78	1500	0300	10/19/78 - 01/30/80
NOAA-6	06/27/79	1930	0730	06/27/79 - 11/16/86
NOAA-7	06/23/81	1430	0230	08/24/81 - 06/07/86
NOAA-8	03/28/83	1930	0730	05/03/83 - 10/31/85
NOAA-9	12/12/84	1420	0220	02/25/85 - Present
NOAA-10	09/17/86	1930	0730	11/17/86 - Present
NOAA-11	09/24/88	1340	0140	11/08/88 - 09/13/94
NOAA-12	05/14/91	1930	0730	05/14/91 - Present
NOAA-14	12/30/94	1340	0140	12/30/94 - Present

Table 11: AVHRR Launch History

[a] NOAA-B launched May 29, 1980, failed to achieve orbit. NOAA-13 launched August 9, 1993, failed due to an electrical short circuit in the solar array.

[b] An ascending node would imply a northbound Equatorial crossing while a descending node would imply a southbound Equatorial crossing.

Data Description The AVHRR sensor provides global (pole to pole) on-board collection of data from all spectral channels. Each pass of the satellite provides a 2399 km wide swath. The satellite orbits the Earth 14 times each day. AVHRR data are acquired in three formats:

High Resolution Picture Transmission (HRPT) data are full resolution image data transmitted to a ground station as they are collected. The average instantaneous field-of-view of 1.4 milliradians yields a HRPT ground resolution of approximately 1.1 km at the satellite nadir from the nominal orbit altitude of 833 km.

Local Area Coverage (LAC) are full resolution data that are recorded on an onboard tape for subsequent transmission during a station overpass. The average instantaneous field-of-view of 1.4 milliradians yields a LAC ground resolution of approximately 1.1 km at the satellite nadir from the nominal orbit altitude of 833 km.

Global Area Coverage (GAC) data are derived from a sample averaging of the full resolution AVHRR data. Four out of every five samples along the scan line are used to compute one average value and the data from only every third scan line are processed, yielding 1.1 km by 4 km resolution at the subpoint.

Future EUMETSAT is currently preparing the European component of a joint European/US polar satellite system. EUMETSAT plans to assume responsibility for the "morning" (local time) orbit and the US will continue with the "afternoon" coverage. It is planned to carry EUMETSAT instruments on the METOP satellite, developed in cooperation with ESA, for a launch in the year 2002. METOP-1 will be the first of a series of operational satellites providing service well into the second decade of the 21st century.

B.2.2 Along Track Scanning Radiometer (ATSR)

The Along Track Scanning Radiometer (ATSR-2) is similar to the AVHRR instrument with the addition of a forward scan at about 55 °. This provides a dual view of the atmosphere although the repeat cycle is reduced to about 3 days (cf. 12 hours for the AVHRR) ATSR/2 senses at six wavelengths (0.56, 0.67, 0.87. 1.6, 11, and 12 μm)with a sub-satellite footprint of about 1 km^2.

Future AATSR is due to launch on ENVISAT-1 in 1999.

B.2.3 Global Ozone Monitoring Experiment (GOME)

GOME is a high resolution (0.2-0.4 nm) spectrometer on board ESA's ERS-2 satellite, launched in April 1995 into a near circular, sun-synchronous orbit. GOME measures the reflected solar radiation from 240 to 800 nm in 3 pixels around nadir (320 km cross track by 40 km along track) and one backscan pixel. Global coverage is achieved once every 3 days. GOME data has been used to deriving the atmospheric aerosol content with the limiting factors being the varying ground surface albedo and clouds.

Future GOME is a pilot project for atmospheric missions such as SCIAMACHY (see later).

B.2.4 Moderate-resolution Imaging Spectroradiometer (MODIS)

The moderate-resolution imaging spectroradiometer (MODIS) is planned to be launched in June 1998 aboard the EOS AM-1 spacecraft and in 2002 aboard EOS PM-1. EOS AM-1 is intended to fly at an altitude of 705 km in a sun-synchronous, near-polar orbit with a 10:30 equator crossing time. PM-1 will have a 1:30 equator crossing time.MODIS is a nadir viewing instrument with 36 spectral bands ranging in wavelength from 0.4 μm to 14.4 μm (see Table 12). Two bands (bands 1-2) are imaged at a nominal resolution of 250 m at nadir, with five bands at 500 m (bands 3-7) and the remaining 29 bands at 1,000 m. A $\pm$55-degree scanning pattern at the EOS orbit achieves a 2,330-km swath and provides global coverage every one to two days.

Primary Use	**Band**	**Bandwidth**
Land/Cloud	1	620 - 670 nm
Boundaries	2	841 - 876 nm
Land/Cloud	3	459 - 479 nm
Properties	4	545 - 565 nm
	5	1230 - 1250 nm
	6	1628 - 1652 nm
	7	2105 - 2155 nm
Ocean Colour/	8	405 - 420 nm
Phytoplankton/	9	438 - 448 nm
Biogeochemistry	10	483 - 493 nm
	11	526 - 536 nm
	12	546 - 556 nm
	13	662 - 672 nm
	14	673 - 683 nm
	15	743 - 753 nm
	16	862 - 877 nm
Atmospheric	17	890 - 920 nm
Water Vapour	18	931 - 941 nm
	19	915 - 965 nm
Surface/Cloud	20	3.660 - 3.840 μm
Temperature	21	3.929 - 3.989 μm
	22	3.929 - 3.989 μm
	23	4.020 - 4.080 μm
Atmospheric	24	4.433 - 4.498 μm
Temperature	25	4.482 - 4.549 μm
Cirrus Clouds	26	1.360 - 1.390 μm
Water Vapour	27	6.535 - 6.895 μm
	28	7.175 - 7.475 μm
	29	8.400 - 8.700 μm
Ozone	30	9.580 - 9.880 μm
Surface/Cloud	31	10.780 - 11.280 μm
Temperature	32	11.770 - 12.270 μm
Cloud Top	33	13.185 - 13.485 μm
Altitude	34	13.485 - 13.785 μm
	35	13.785 - 14.085 μm

Table 12: MODIS Spectral Bands.

B.2.5 Operational Linescan System (OLS)

The Operational Linescan System (OLS) is carried on the Defense Meteorological Program (DMSP) spacecraft (currently Block 5D-2). At any one time two operational Block 5D-2 satellites are in a a near polar sun synchronous orbit (currently 0536 and 1052 local time) at an altitude of approximately 830 km above the earth. Each satellite crosses any point on the earth twice a day and has an orbital period of about 101 minutes thus providing complete global coverage every six hours. The OLS instrument consists of a visible (0.58 - 0.91 μm) and an infrared (10.3 - 12.9 μm) sensor during the day. At night a photo multiplier tube (0.47 - 0.95 μm) is substituted for the visible channel. The telescope channels provide a high resolution (0.5 km) which can be down-graded to 2.7 km by averaging 25 pixels. The PMT resolution is 2.7 km. The next generation of Defense Meteorological Satellite Program spacecraft, Block 5D-3, is expected to be launched in 1999.

B.2.6 Total Ozone Mapping Spectrometer (TOMS)

The Total Ozone Mapping Spectrometer (TOMS) is a nadir viewing instrument which has operated on four platforms since 1978 (currently Earth Probe TOMS). TOMS operates by comparing incident solar radiation with radiation reflected from Earth's atmosphere in six UV wavebands (380, 360, 340, 331, 318 and 313 nm) each with a bandwidth of 1 nm. TOMS has a 50 $\times$ 50 km nadir field of view increasing to 125 $\times$ 280 km at the extreme of the scan angle. The primary purpose of TOMS is to measure atmospheric ozone however it is also sensitive to the large amounts of SO_2 injected into the stratosphere by volcanic eruptions which absorb at some of the same frequencies of ozone.

NASA/GSFC are already providing TOMS realtime and near realtime SO_2 and ozone data in several forms.

1. The Earth Probe TOMS data are collected directly from the satellite in real time by stations in Alaska (NWS Anchorage) and McMurdo (NSF) to provide local coverage. The time delay in this case is about a minute to batch process the 5 - 15 minutes of overpass data for the 4 - 14 orbits that can be seen from these ground stations. The objective of the Alaska experiment is to provide warnings to aircraft through the FAA Air Traffic Control Center.

2. The orbital Earth Probe TOMS data are collected at Wallops in 2 daily dumps and processed immediately at GSFC for global coverage. The time delay is about 12 hours for the oldest data. NOAA/NESDIS is planning to use the SO_2 data for aircraft hazards. NESDIS is planning to use this source of data for hazard warnings later this year.

TOMS is capable of detecting volcanic ash clouds (Seftor et al., 1997) from the spectral contrast between its two channels at 340 and 380 nm.

B.3 Low Earth Orbit: Limb Viewing Instruments - Occultation

B.3.1 Global Ozone Monitoring By Occultations Of Stars (GOMOS)

The Global Ozone Monitoring By Occultations Of Stars (GOMOS) experiment consisting of two spectrometers (UV-visible, infrared) and two photometers (visible) is scheduled for launch on Envisat-1 in 1998. The main scientific objective of GOMOS is to monitor ozone and ozone trends in the Stratosphere and Mesosphere. This task is achieved by measuring stellar spectra in the UV to near-infrared range while stars are being eclipsed by the Earth. The GOMOS observing strategy is a limb viewing mode between altitudes 10 km to 100 km. The vertical resolution will be about 1.7 km. About 25 stars (magnitudes between -1 and 3) will be monitored each orbit.

B.3.2 Stratospheric Aerosol and Gas Experiment (SAGE) III

Operational The Stratospheric Aerosol and Gas Experiment (SAGE) III is scheduled for launch in August 1998 and will use solar occultation (385, 430-450, 525, 740-780, 920-960, 1020, 1550 nm) and lunar occultation (at 430-450, 740-780, 920-960 nm) to measure atmospheric profiles of trace gases and aerosols.

B.4 Low Earth Orbit: Limb Viewing Instruments - Atmospheric Emission

B.4.1 The High Resolution Dynamics Limb Sounder (HIRDLS)

The High Resolution Dynamics Limb Sounder (HIRDLS) is an infra-red limb scanning radiometer which will be part of the NASA EOS Chem-1 payload to be launched in 2002. HIRDLS is designed to sound the upper troposphere, stratosphere, and mesosphere in order to measure temperature, geopotential height gradients and concentrations of O_3, H_2O, CH_4, N_2O, NO_2, HNO_3, N_2O_5, $ClONO_2$, $CFCl_3$, CF_2Cl_2, aerosol amounts, locations of polar stratospheric clouds and cloud-top heights. HIRDLS performs limb scans in the vertical at multiple azimuth angles, measuring infra-red emissions in 21 channels ranging from 6.12 to 17.6 μm(see Table 13). High vertical resolution will be obtained by using a 1 km vertical field of view with multiple oversampling. The multispectral capability should enable ash clouds to be discriminated from water/ice clouds, with the advantage that cold space provides a strongly contrasting background so that the measurement will not be confused by cloud at lower altitudes. A disadvantage is that the technique cannot see through tropospheric cloud. The satellite will be in a polar orbit, and will measure a swath of profiles along the track, on an approximately 500 km $\times$ 500 km grid. It is planned to carry an instrument like TOMS on Chem-1. This will be sensitive to SO_2 when in large concentrations.

Channel	Target Species	Band (μm)
1	N_2O, aerosol	17.01 – 17.76
2	CO_2	16.26 – 16.67
3	CO_2	15.63 – 16.39
4	CO_2	15.15 – 15.97
5	CO_2	14.71 – 15.27
6	aerosol	11.96 – 12.18
7	$CFCl_3$	11.72 – 11.98
8	HNO_3	11.05 – 11.63
9	CF_2Cl_2	10.72 – 10.93
10	O_3	9.90 – 10.10
11	O_3	9.54 – 9.89
12	O_3	8.77 – 8.93
13	aerosol	8.20 – 8.33
14	N_2O_5	7.94 – 8.14
15	N_2O	7.80 – 7.96
16	$ClONO_2$	7.70 – 7.82
17	CH_4	7.30 – 7.55
18	H_2O	6.97 – 7.22
19	aerosol	7.06 – 7.13
20	H_2O	6.49 – 7.03
21	NO_2	6.12 – 6.32

Table 13: HIRDLS Spectral Bands.

B.4.2 Michelson Interferometer for Passive Atmospheric Sounding (MIPAS)

The Michelson Interferometer for Passive Atmospheric Sounding (MIPAS) is a high resolution Fourier transform spectrometer due to be launched in 1998 on Envisat-1. The Michelson Interferometer of MIPAS operates

in the wavelength range 4.15 – 14.6 μm. The limb measurements can be performed either in rearward or sideways viewing directions. The former is the nominal viewing geometry while the latter might be used for special events (e.g. volcanic eruptions). The MIPAS observation 'footprint' for an atmosphere measurement is approximately a box 3 km thick, 392 km along the line-of-sight and 30 km wide centred on the tangent point. Figure 7 shows the MIPAS scan pattern for one day represented by $\pm$196 km vectors centred on the tangent point along the line-of-sight. Although global coverage is obtained within 12 hours, the sampling of all atmospheric locations takes several days.

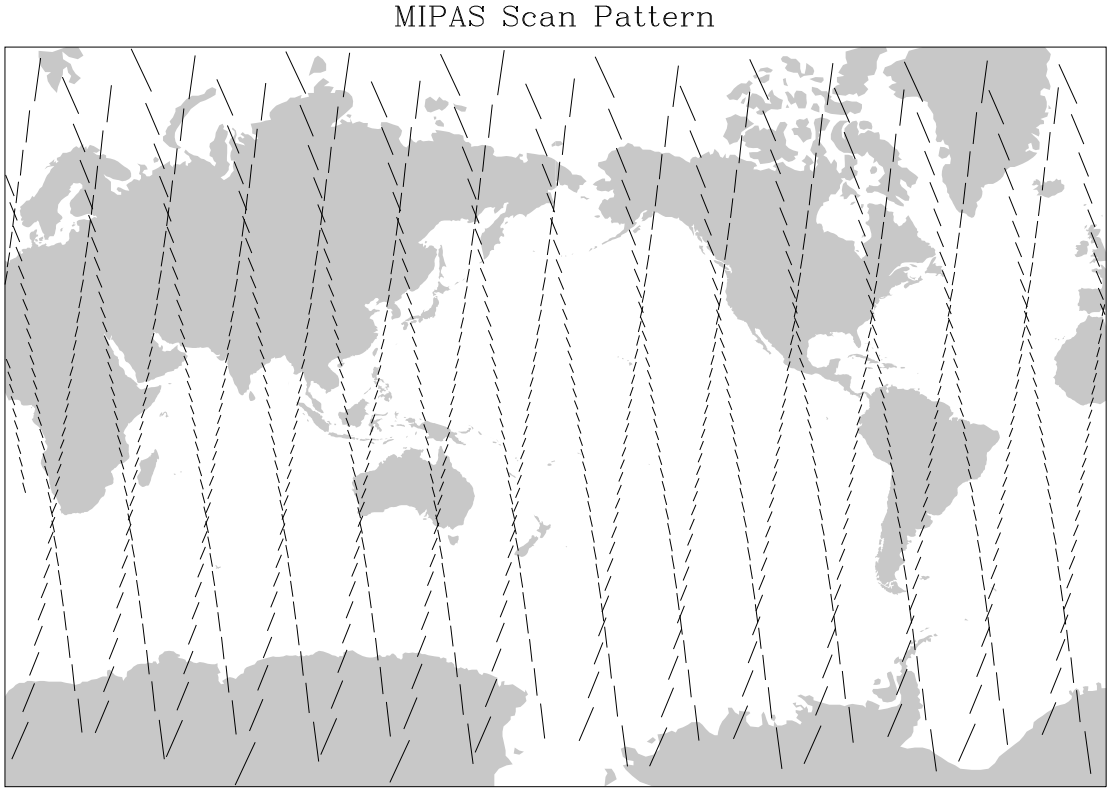

Figure 7: Line-of-sight vectors centered on the MIPAS tangent point for a typical 1 day observation sequence.

B.4.3 Scanning Imaging Absorption Spectrometer For Atmospheric Chartography (SCIAMACHY)

The Scanning Imaging Absorption Spectrometer For Atmospheric Chartography (SCIAMACHY) is due to fly on ENVISAT-1 and will measure atmospheric absorption spectra in spectral bands from the UV to the near infrared using reflected solar radiation. SCIAMACHY will view the atmosphere either in nadir scanning mode or limb scanning mode. In nadir mode, an area of 500 km to either side of nadir is scanned across track. By setting the minimum exposure time, the achieved across-track resolution will amount to 16 km. In limb mode, SCIAMACHY scans horizontally sequential atmospheric layers of 1000 km x 1.3 km size within an altitude range of 0 km - 100 km. In addition to observations of the atmosphere in reflected and backscattered sunlight, SCIAMACHY is also capable of performing measurements of Solar and Lunar occultations (at the Earth's horizon). Particularly during Sun occultations, the high signal-to-noise ratio will allow short exposure times, thus leading to spectral information with high spatial resolution. Global coverage will be obtained in 3 days.

References

Barquero, J., Volcanoes and aviation safety in Costa Rica, in *Volcanic Ash And Aviation Safety*, Proc. 1st Int. Symp. on Volcanic Ash and Aviation Safety, Ed. T.J. Casadevall, USGS Bull. 2047, 1994.

Bayhurst, G.K., K.H. Wohletz and A.S. Mason, A method for characterizing volcanic ash from the December 15, 1989 eruption of Redoubt volcano, Alaska, in *Volcanic Ash And Aviation Safety*, Proc. 1st Int. Symp. on Volcanic Ash and Aviation Safety, Ed. T.J. Casadevall, USGS Bull. 2047, 1994.

Bluth, G.J.S, S.D. Doiron, C.C. Schnetzler, A.J. Krueger and L. S. Walter, Global tracking of the SO_2 clouds from the June, 1991, Mount Pinatubo Eruptions, *Geophysical Research Letters*, **19**, 151–154, 1992.

Brantley, S.R. (Ed.), *The Eruption Of Redoubt Volcano, Alaska December 14, 1989-August 31, 1990*, USGS Circ. 1061, 1990.

Bursik, M.I., R.S.J. Sparks, S.N. Carey and J.S. Gilbert, The concentration of ash in volcanic plumes, inferred from dispersal data, in *Volcanic Ash And Aviation Safety*, Proc. 1st Int. Symp. on Volcanic Ash and Aviation Safety, Ed. T.J. Casadevall, USGS Bull. 2047, 1994.

Campbell, E.E., Recommended flight-crew procedures if volcanic ash is encountered, in *Volcanic Ash And Aviation Safety*, Proc. 1st Int. Symp. on Volcanic Ash and Aviation Safety, Ed. T.J. Casadevall, USGS Bull. 2047, 1994.

Casadevall, T.J. (Ed.), Introduction to *Volcanic Ash And Aviation Safety*, Proc. 1st Int. Symp. on Volcanic Ash and Aviation Safety, USGS Bull. 2047, 1994.

Deirmendjian, D., *Electromagnetic Scattering On Spherical Polydispersions*, Elsevier, 1969.

Dunn, M.G. and D.P. Wade, Influence of volcanic ash clouds on gas turbine engines, in *Volcanic Ash And Aviation Safety*, Proc. 1st Int. Symp. on Volcanic Ash and Aviation Safety, Ed. T.J. Casadevall, USGS Bull. 2047, 1994.

Farlow, N.H., V.R. Oberbeck, K.G. Snetsinger, G.V. Ferry, G. Polkowski and D.M. Hayes, Size distributions and mineralogy of ash particles in the stratosphere from eruptions of Mount St. Helens, , **211**, 830–832, 1981.

FISHER, R.V. AND H.-U. SCHMINCKE, VOLCANICLASTIC SEDIMENT TRANSPORT AND DEPOSITION. IN *Sediment Transport And Depositional Processes*, ED. K. PYE, CAMBRIDGE, BLACKWELL SCIENTIFIC PUBLICATIONS, 351–388, 1994.

GOODING, J.L., U.S. CLANTON, E.M. GABEL AND J.L. WARREN, EL CHICHÓN VOLCANIC ASH IN THE STRATOSPHERE: PARTICLE ABUNDANCES AND SIZE DISTRIBUTIONS AFTER THE 1982 ERUPTION, *Geophysical Research Letters*, **10**, 1033–1036, 1983.

GRAINGER, R.G., *The Calculation Of Cloud Parameters Using AVHRR Data*, PHD THESIS, UNIVERSITY OF AUCKLAND, 1990.

GRAINGER R. G., A. LAMBERT, F. W. TAYLOR, J. J. REMEDIOS, C. D. RODGERS, M. CORNEY AND B. J. KERRIDGE, INFRARED ABSORPTION BY VOLCANIC STRATOSPHERIC AEROSOLS OBSERVED BY ISAMS, *Geophysical Research Letters*, **20**, 1283–1286, 1993.

HARRIS, D.M. AND W.I. ROSE JR, ESTIMATING PARTICLE SIZES, CONCENTRATIONS AND TOTAL MASS OF ASH IN VOLCANIC CLOUDS USING WEATHER RADAR, *Journal of Geophysical Research*, **88**, 10969–10983, 1983.

HARRIS, A.J., R.A. VAUGHAN AND D.A.ROTHERY, VOLCANO DETECTION AND MONITORING USING AVHRR DATA: THE KRAFLA ERUPTION, 1984, *International Journal of Remote Sensing*, **16**, 1001–1020, 1995.

HEIKEN, G., VOLCANIC ASH: WHAT IT IS AND HOW IT FORMS, IN *Volcanic Ash And Aviation Safety*, PROC. 1ST INT. SYMP. ON VOLCANIC ASH AND AVIATION SAFETY, ED. T.J. CASADEVALL, USGS BULL. 2047, 1994.

HOBBS, P.V., L.F. RADKE, J.H. LYONS, R.J. FEREK, D.J. COFFMAN AND T.J. CASADEVALL, AIRBORNE MEASUREMENTS OF PARTICLE AND GAS EMISSIONS FROM THE 1990 VOLCANIC ERUPTIONS OF MT REDOUBT, *Journal of Geophysical Research*, **96**, 18735–18752, 1991.

HOLASEK, R.E. AND W.I. ROSE, ANATOMY OF 1986 AUGUSTINE VOLCANO ERUPTIONS AS RECORDED BY MULTISPECTRAL IMAGE PROCESSING OF DIGITAL AVHRR WEATHER SATELLITE DATA, *Bulletin of Volcanology*, **53**, 420-435, 1991.

HOLASEK, R.E., S. SELF AND A.W. WOODS, SATELLITE OBSERVATIONS AND INTERPRETATION OF THE 1991 MOUNT PINATUBO ERUPTION PLUMES, *Journal of Geophysical Research*, **101**, 27635–27655, 1996.

KIDWELL, K.B. (ED.), *NOAA Polar Orbiter Data (TIROS-N, NOAA-6, NOAA-7, NOAA-8, NOAA-9, NOAA-10, NOAA-11, NOAA-12, and NOAA-14) Users Guide*, NOAA/NESDIS, WASHINGTON, D.C., 1995.

KERDILES, H. AND R. DIAZ, MAPPING OF THE VOLCANIC ASHES FROM THE 1991 HUDSON ERUPTION USING NOAA-AVHRR DATA, *International Journal of Remote Sensing*, **17**, 1981–1995, 1996.

KNOLLENBERG, R.G. AND D. HUFFMAN, MEASUREMENTS OF THE AEROSOL SIZE DISTRIBUTIONS OF THE EL CHICHON CLOUD, *Geophysical Research Letters*, **10**, 1025–1028, 1983.

MACKINNON, I.D. R., J.L. GOODING, D.S. MCKAY AND U.S. CLANTON, THE EL CHICHÓN STRATOSPHERIC CLOUD, SOLID PARTICULATES AND SETTLING RATES, *Journal of Volcanology and Geothermal Research*, **23**, 125–146, 1984.

MACEDONIO, G., P. PAPALE, M.T. PARESCHI, M. ROSI AND R. SANTACROCE, ASTATISTICAL APPROACH TO THE ASSESSMENT OF VOLCANIC HAZARD FOR AIR TRAFFIC: APPLICATION TO VERSUVIUS, ITALY, IN *Volcanic Ash And Aviation Safety*, PROC. 1ST INT. SYMP. ON VOLCANIC ASH AND AVIATION SAFETY, ED. T.J. CASADEVALL, USGS BULL. 2047, 1994.

MATSON, M., THE 1982 EL CHICHÓN VOLCANO ERUPTIONS - A SATELLITE PERSPECTIVE, *Journal of Volcanology and Geothermal Research*, **23**, 1–10, 1984.

PALMER, K.F. AND D. WILLIAMS, OPTICAL CONSTANTS OF SULFURIC ACID, APPLICATION TO THE CLOUDS OF VENUS? *Applied Optics*, **14**, 208–219, 1975.

READ, W., L. FROIDEVAUX AND J. WATERS, MICROWAVE LIMB SOUNDER MEASUREMENTS OF STRATOSPHERIC SO_2 FROM THE MT PINATUBO VOLCANO, *Journal of Geophysical Research*, **20**, 1299–1302, 1993.

PRATA, A.J., INFRARED RADIATIVE TRANSFER CALCULATIONS FOR VOLCANIC ASH CLOUDS, *Geophysical Research Letters*, **16**, 1293–1296, 1989.

ROSE, W.I., D.J. DELENE, D.J. SCHNEIDER, G.J.S. BLUTH, A.J. KRUEGER, I. SPROD, C. MCKEE, H.L. DAVIES AND G.G.J. ERNST, ICE IN THE 1994 RABAUL ERUPTION CLOUD: IMPLICATIONS FOR VOLCANO HAZARD AND ATMOSPHERIC EFFECTS, *Nature*, 375, 477–479, 1995.

SAWADWA, Y, TRACKING OF REGIONAL VOLCANIC ASH CLOUDS BY GEOSTATIONARY METEOROLOGICAL SATELLITE (GMS), IN *Volcanic Ash And Aviation Safety*, PROC. 1ST INT. SYMP. ON VOLCANIC ASH AND AVIATION SAFETY, ED. T.J. CASADEVALL, USGS BULL. 2047, 1994.

SEFTOR, C.J., N.C. HSU, J.R. HERMAN, P.K. BHARTIA, O. TORRES, W.I. ROSE, D.J. SCHNEIDER AND N. KROTKOV, DETECTION OF VOLCANIC ASH CLOUDS FROM NIMBUS 7 / TOTAL OZONE MAPPING SPECTROMETER, *Journal of Geophysical Research*, **102**, 16749–16759, 1997.

SELF, S. AND G.P.L. WALKER, ASH CLOUDS: CHARACTERISTICS OF ERUPTION COLUMNS, IN *Volcanic Ash And Aviation Safety*, PROC. 1ST INT. SYMP. ON VOLCANIC ASH AND AVIATION SAFETY, ED. T.J. CASADEVALL, USGS BULL. 2047, 1994.

SIMKIN, T., AND L. SIEBERT, *Volcanoes Of The World*, 2ND EDITION: TUCSON, GEOSCIENCE PRESS, 349P, 1994.

SPARKS, R.S.J., M.I. BURSIK, S.N. CAREY, A.W. WOODS AND J.S. GILBERT, THE CONTROLS OF ERUPTION-COLUMN DYNAMICS ON THE INJECTION AND MASS LOADING OF ASH INTO THE ATMOSPHERE, IN *Volcanic Ash And Aviation Safety*, PROC. 1ST INT. SYMP. ON VOLCANIC ASH AND AVIATION SAFETY, ED. T.J. CASADEVALL, USGS BULL. 2047, 1994.

SWANSON, S.E. AND J.E. BEGET, MELTING PROPERTIES OF VOLCANIC ASH, IN *Volcanic Ash And Aviation Safety*, PROC. 1ST INT. SYMP. ON VOLCANIC ASH AND AVIATION SAFETY, ED. T.J. CASADEVALL, USGS BULL. 2047, 1994.

TOON, O.B., M.A. TOLBERT, B.G. KOEHLER, A.M. MIDDLEBROOK AND J. JORDAN, INFRARED OPTICAL CONSTANTS OF H_2O ICE, AMORPHOUS NITRIC ACID SOLUTIONS AND NITRIC ACID HYDRATES, *Journal of Geophysical Research*, **99**, 25631–25654, 1994.

WEM, S. AND W. I. ROSE, RETRIEVAL OF SIZES AND TOTAL MASSES OF PARTICLES IN VOLCANIC CLOUDS USING AVHRR BANDS 4 AND 5, *Journal of Geophysical Research*, **99**, 5421–5431, 1994.

WOODS, A. W. AND J. KIENLE, THE INJECTION OF VOLCANIC ASH INTO THE ATMOSPHERE, IN *Volcanic Ash And Aviation Safety*, PROC. 1ST INT. SYMP. ON VOLCANIC ASH AND AVIATION SAFETY, ED. T.J. CASADEVALL, USGS BULL. 2047, 1994.

WRIGHT, T.L. AND T.C. PIERSON, *Living With Volcanoes*, USGS CIRC, 1992.

VOLZ, F.E., INFRARED OPTICAL CONSTANTS OF AMMONIUM SULFATE, SAHARA DUST, VOLCANIC PUMICE AND FLYASH, *Applied Optics*, **12**, 564–568, 1973.